Nanophotonics 2020; 9(14): 4295–4306

Research article

Nannan Xu, Haifeng Wang, Huanian Zhang*, Linguang Guo, Xinxin Shang, Shouzhen Jiang and Dengwang Li*

Palladium diselenide as a direct absorption saturable absorber for ultrafast mode-locked operations: from all anomalous dispersion to all normal dispersion

https://doi.org/10.1515/nanoph-2020-0267
Received May 4, 2020; accepted July 14, 2020; published online July 28, 2020

Abstract: Layered transition metal dichalcogenides with excellent nonlinear absorption properties have shown remarkable performance in acting as ultrafast photonics devices. In our work, palladium diselenide ($PdSe_2$) nanosheets with competitive advantages of wide tunable bandgap, unique puckered pentagonal structure and excellent air stability are prepared by the liquid-phase exfoliation method. Its ultrafast absorption performance was verified by demonstrating conventional and dissipative soliton operations within Er-doped fiber lasers. The minimum pulse width of the conventional soliton was 1.19 ps. Meanwhile, dissipative soliton with a 46.67 mW output power, 35.37 nm spectrum width, 14.92 ps pulse width and 2.86 nJ pulse energy was also generated successfully. Our enhanced experiment results present the excellent absorption performance of $PdSe_2$ and highlight the capacity of $PdSe_2$ in acting as ultrafast photonics devices.

Keywords: dissipative soliton; large-energy mode-locked lasers; palladium diselenide; ultrafast modulation application.

Nannan Xu and Haifeng Wang: These authors equally contributed to this work.

***Corresponding authors: Huanian Zhang**, Shandong Key Laboratory of Medical Physics and Image Processing, Shandong Institute of Industrial Technology for Health Sciences and Precision Medicine, School of Physics and Electronics, Shandong Normal University, Jinan, Shandong 250358, China; School of Physics and Optoelectronic Engineering, Shandong University of Technology, Zibo 255049, China, E-mail: huanian_zhang@163.com; and **Dengwang Li**, Shandong Key Laboratory of Medical Physics and Image Processing, Shandong Institute of Industrial Technology for Health Sciences and Precision Medicine, School of Physics and Electronics, Shandong Normal University, Jinan, Shandong 250358, China, dengwang@sdnu.edu.cn, https://orcid.org/0000-0001-7369-3379 (H. Zhang)
Nannan Xu, Linguang Guo, Xinxin Shang and Shouzhen Jiang: Shandong Key Laboratory of Medical Physics and Image Processing, Shandong Institute of Industrial Technology for Health Sciences and Precision Medicine, School of Physics and Electronics, Shandong Normal University, Jinan, Shandong 250358, China
Haifeng Wang: Department of Physics, College of Science, Shihezi University, Xinjiang 832003, China

1 Introduction

Ultrafast mode-locked fiber lasers have been widely investigated owing to their extensive applications in communication, biophotonics, photochemistry and so on [1–4]. Hitherto, active and passive mode-locked technologies have been widely employed to achieve ultrafast mode-locked operations. Compared with active mode-locked method, passive mode-locked technology is well-known due to their properties of environmental stability, alignment-free and compact design without modulators required [5, 6]. Currently, a variety of saturable absorbers (SAs) such as single-walled carbon nanotubes [7–9], semiconductor saturable absorber mirrors [10, 11], graphene [12–15], graphene oxide [16] and quantum dots (QDs) [6, 7] have been extensively investigated for generating mode-locked fiber lasers. Especially, graphene has enormously promoted the development of mode-locked lasers due to its properties of wide absorption range, low saturation intensity, ultrafast recovery time and high damage threshold [12–15]. Under the encouragement of graphene, similar findings in other 2D nanomaterials such as topological insulators (TIs) [17–20], transition metal dichalcogenides (TMDs) [21–34], black phosphorus [35–37], MXenes [38, 39], Xenes [40–45] and so on have been reported focusing their saturable absorption and laser propagation performance. Among them, TMDs exhibit significant essential applications in optoelectronic and biological fields [46–48]. In 2013, MoS_2, as a typical TMD material, was found possessing excellent saturable absorption behavior by Wang et al. [48]. Since then, TMDs were widely used for constructing ultrafast mode-lock lasers [21–34] due to their excellent nonlinear optical properties and absorption performance.

TMDs can be expressed with the formula MX_2, in which M represents transition metals (M = Mo, W, Ta, Pd, Nb, Re, Ti, etc.) and X is chalcogen (X = S, Se, Te). In our work, palladium diselenide ($PdSe_2$), a novel TMD with wide tunable bandgap and high room temperature mobility [49, 50], is introduced as a promising 2D ultrafast photonics material. In comparison with common reported TMDs, $PdSe_2$ exhibits the most competitive properties of wide tunable bandgap value varying from 0 (bulk) to 1.3 eV (monolayer) [51], with a bandgap shift of 0.2 eV between monolayer and bilayer in the material [52]. Such a wide tunable bandgap indicates that $PdSe_2$ can be employed for designing direct absorption ultrafast photonics devices with wide absorption band, which is rarely demonstrated in other 2D materials. As is reported by Puretzky et al. [53], the origin of the wide tunable bandgap in $PdSe_2$ is due to the strong interlayer coupling in $Pdse_2$ compared to other 2D materials. In addition, the unit cell of bulk $PdSe_2$ is composed with the space group P_{bca} (no. 61) and D_{2h} point group symmetry in an orthorhombic structure [54]. Compared to the previous investigated layered TMDs, as is shown in Figure 1a, the most remarkable difference is that each palladium atom in $PdSe_2$ is coordinated with four selenium atoms, forming a unique puckered pentagonal structure, unlike the six coordinated transition metal atoms in typical T- or H-phase structures [55]. Pentagonal 2D materials were firstly demonstrated by the discovery of penta-graphene. Since then, $PdSe_2$, PdS_2 [56], B_2C [57], SiC_2 [58], SiH [59], AlN_2 [60] and so on have emerged with the unique pentagonal structure. Unlike reported hexagonal structure, the pentagonal conduction band minimum is not situated along the high symmetry lines in the first Brillouin zone, which constitute the low symmetry structure and leads to the notable optical properties of anisotropic behavior [49, 61, 62]. The anisotropy caused by pentagonal structure provides an essential physical basis for the design of novel diversified photonics devices. Oyedele [62] also found that a phase transformation in a region of $PdSe_2$ can lead to the formation of seamless Ohmic contacts for field-effect transistors, which opens new possibilities in the development of better electrical contacts for practical applications of 2D materials. Besides, they also proved that $PdSe_2$ had outstanding air stability property, which was demonstrated by exposing $PdSe_2$ in air for 60 days [50]. It is well known that excellent air stability property exhibits great significance in expending the practical applications of 2D material–based devices. Recently high quality $PdSe_2$ materials have also been successfully prepared by the chemical vapor deposition method and a hybrid method of top-down and bottom-up processes, showing great significance in designing novel practical optoelectronic devices [63, 64]. So far, $PdSe_2$-based devices including a field-effect transistor with tunable ambipolar characteristics and a highly sensitive, air-stable infrared photodetector have been demonstrated successfully [54, 55]. However, the ultrafast nonlinear optical properties of $PdSe_2$ are awaiting further investigations. Exploring the ultrafast applications of $PdSe_2$ will promote the development of efficient 2D material–based photonics devices.

In this paper, layer-dependent electronic structures and bandgap characteristics of $PdSe_2$ were calculated for better guiding the design of $PdSe_2$-based ultrafast photonics devices. Based on the theoretical guidance, a $PdSe_2$ SA with a saturation intensity of 22.67 MW/cm^2 and a modulation depth of 6.2% was prepared and used for obtaining conventional soliton and dissipative soliton operations. For the conventional mode-locked soliton operation, the pulse duration was 1.19 ps with a pulse repetition rate of 7.71 MHz. The dissipative solitons were achieved at the central wavelength of 1560.67 nm with a spectrum width of 35.37 nm, and the pulse width was 14.92 ps with a pulse repetition rate of 16.29 MHz. The theoretical and experimental results all prove that $PdSe_2$ was a good candidate in the field of ultrafast optics with excellent saturable absorption characteristics.

2 Density function theory calculation

In our contribution, for better guiding the preparation of $PdSe_2$-based ultrafast photonics devices, layer-dependent electronic structures and bandgap characteristics of $PdSe_2$ were calculated by using the density function theory and the Vienna Ab initio Simulation Package (VASP) [65–68]. During the calculation, optimized gradient-corrected exchange-correlation functional due to Perdew, Burke, and Ernzerhof (optPBE) implemented in VASP were employed due to its reasonable calculated results for structural and electronic and properties [67, 68]. The energy cutoff for the

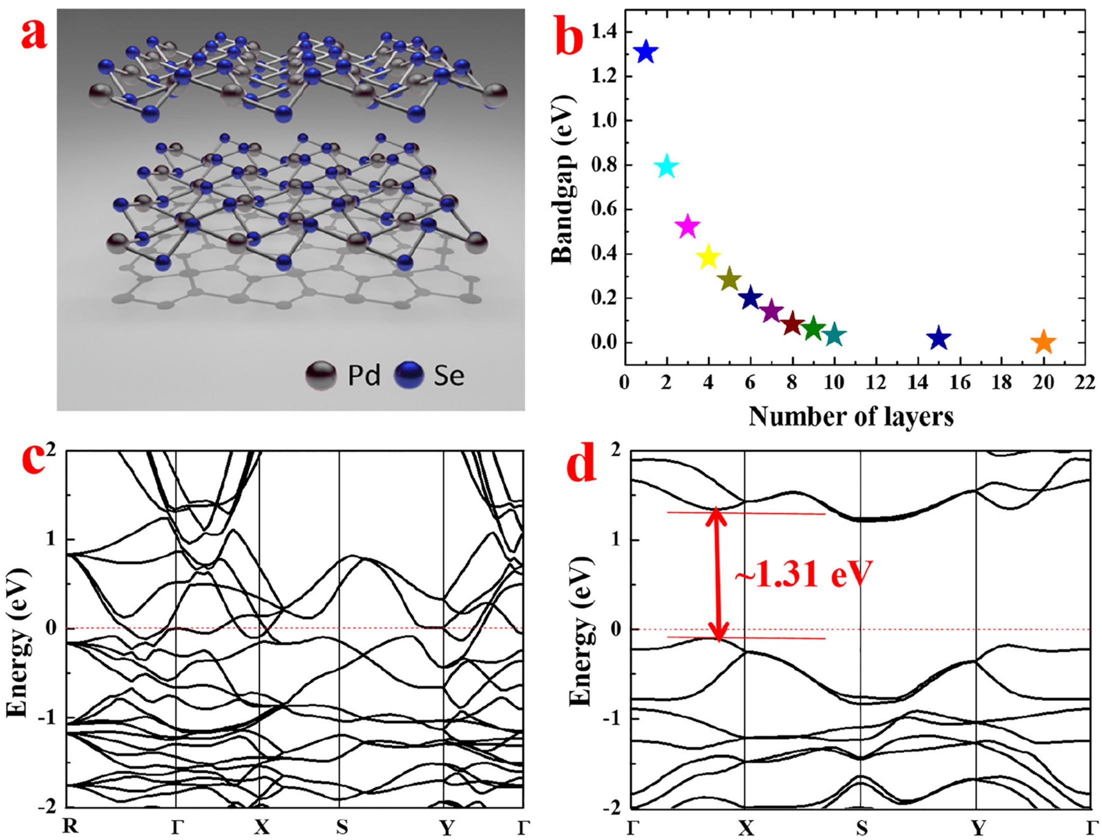

Figure 1: (a) Atomic structures of $PdSe_2$. (b) The bandgap characteristics of $PdSe_2$ vs. its layer number. (c) Calculated electronic band structure of bulk $PdSe_2$. (d) Calculated electronic band structure of single-layered $PdSe_2$. $PdSe_2$, palladium diselenide.

plane-wave basis and the k-point spacing of the reciprocal space were set to 500 eV and 0.02 $Å^{-1}$, respectively. In addition, all atoms were relaxed until the residual forces were below 0.001 eV/Å. For the 2D slab calculations (monolayer and few-layer $PdSe_2$ systems), a vacuum region of at least 20 Å in the out-of-plane direction was used to avoid spurious interactions with periodic images. The calculated results are provided in Figure 1. As is shown in Figure 1b, with the increasing of the number of layers, the bandgap value decreases from about 1.31 eV (single-layer $PdSe_2$) to −0.01 eV (bulk $PdSe_2$). Meanwhile, the accurate calculated bandgap value of 2, 5, 10, 15 and 20 layer $PdSe_2$ is 0.79, 0.28, 0.03, 0.02 and 0 eV, respectively. Additionally, the calculated electronic band structures of bulk and single-layer $PdSe_2$ are provided in Figure 1(c) and (d), respectively. Obviously, for the bulk $PdSe_2$, the bandgap is about 0 eV, also indicating that bulk $PdSe_2$ exhibits no bandgap value. However, single-layer $PdSe_2$ exhibits a obvious indirect bandgap of about 1.31 eV, approaching to its direct bandgap of 1.43 eV. In conclusion, the calculated results prove that $PdSe_2$ has a wide tunable bandgap value and exhibit essential significance in guiding the design of $PdSe_2$-based broadband ultrafast photonics devices.

3 The preparation and characterization of $PdSe_2$-based SAs

The preparation process of the $PdSe_2$ SA is displayed in Figure 2. Firstly, $PdSe_2$ solution is prepared with a liquid-phase exfoliation (LPE) method. As shown, 0.1 g $PdSe_2$ powder is added into 100 ml alcohol (30%). After soaking for 48 h, the mixture is then placed in a high-power ultrasonic cleaner (JP-040, Jiemeng, Shenzhen, China) for 6 h (S1). After centrifuging at a speed of 2000 rpm for 30 min (S2), solution with layered $PdSe_2$ nanosheets is obtained. Next, 4 wt% polyvinyl alcohol (PVA) solution is added into the $PdSe_2$ mixture solution at a volume ratio of 3:4 (S3). Uniform $PdSe_2$-PVA dispersion solution is prepared successfully after placing the mixture in the ultrasonic cleaner for another 4 h. Secondly, $PdSe_2$-based SA is prepared by employing the $PdSe_2$-PVA dispersion solution and a piece of tapered fiber. As provided, 80 µl $PdSe_2$-PVA dispersion solution is coated on the tapered area of the fiber fixed on the glass. After that, the coated tapered fiber is placed into

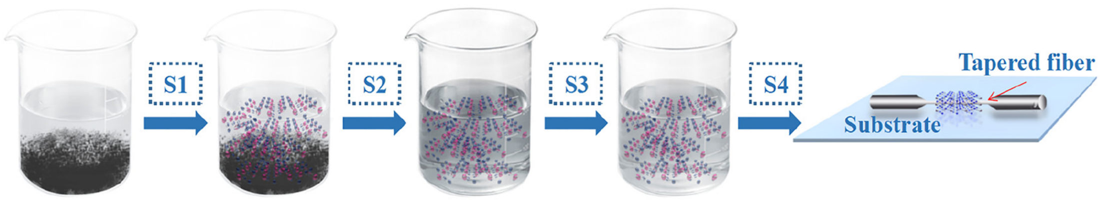

Figure 2: Preparation process of the $PdSe_2$ SA. SA, saturable absorber.

a oven for 48 h at 20 °C. Finally, the $PdSe_2$-based SA is prepared successfully.

During the preparation of the $PdSe_2$ SA, characterization methods including Raman spectrum, transmission electron microscope (TEM) and atomic force microscope (AFM) were used for characterizing the layered structure and thickness characteristics. Firstly, the Raman spectrum of the $PdSe_2$ nanosheet was measured by a Raman spectrometer (Horiba HR Evolution, HORIBA JY, Paris, France). As described in Figure 3(a), four distinct Raman shift peaks at 141.6, 204.3, 221.1 and 253.3 cm^{-1} are recorded, corresponding to the A^1_g, A^2_g, B_{1g} and A^3_g mode of the $PdSe_2$, respectively [50, 51]. No other Raman shifts are observed in the spectrum, indicating that pure $PdSe_2$ material is prepared in our work. Figure 3(b) shows the TEM image of the $PdSe_2$ nanosheets, which was recorded by a JEM-2100 (JEOL, Tokyo, Japan) microscope with an optical resolution of 20 nm. The photography reveals that the $PdSe_2$ nanosheets exhibit obvious layered structures. Figure 3(c) and (d) present the high-resolution TEM images recorded with resolutions of 10 and 2 nm, respectively. Clear crystal lattice with a d-spacing of ~0.4 nm is shown in Figure 3(d), which indicates that $PdSe_2$ nanosheets with high crystallinity are obtained through the LPE method. As is calculated in the theoretical part, the thickness characteristics have great significance in understanding thickness-dependent nonlinear optical properties and designing $PdSe_2$-based ultrafast optical devices. The thickness characteristics are recorded by an atomic force microscope (Bruker Multimode 8, Bruker, Karlsruhe, Germany) and depicted in Figure 3(e). Besides, the corresponding thicknesses of the marked areas of Figure 3(e) are provided in Figure 3(f). The thicknesses of the $PdSe_2$ are about 6 nm, corresponding to ~15–16 layers.

Transmittance curves of the PVA and PVA-$PdSe_2$ SA are provided in Figure 4(a). As is shown, at 1560 nm, the transmittance (T) of the PVA and PVA-$PdSe_2$ SA is 90% and 56%, respectively. The PVA-$PdSe_2$ SA exhibits obvious linear absorption. Additionally, the nonlinear absorption performance of the $PdSe_2$ SA was investigated by a power-

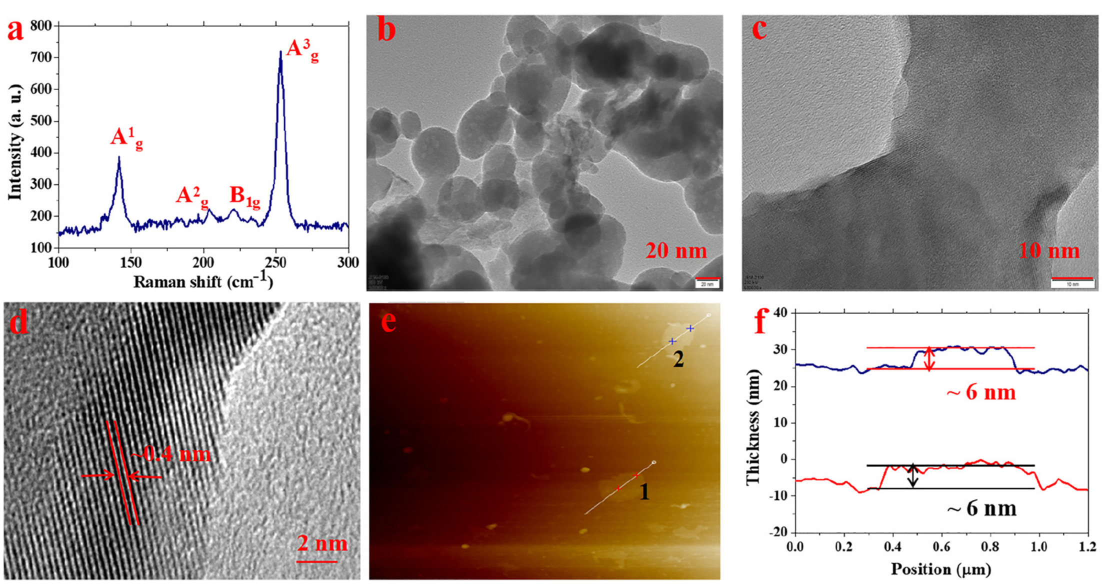

Figure 3: (a) Raman spectrum of the $PdSe_2$ powder. (b) TEM image of the $PdSe_2$ nanosheets. (c) HRTEM image of the $PdSe_2$ nanosheets under the resolution of 10 nm. (d) HRTEM image with obvious crystal lattice. (e) AFM image of the $PdSe_2$ nanosheets. (f) Corresponding thickness characteristics of the marked areas in (e). $PdSe_2$, palladium diselenide; TEM, transmission electron microscope; AFM, atomic force microscope; HRTEM, high-resolution TEM.

dependent transmission technique. The testing platform is provided in the insert of Figure 4. As is depicted, the $PdSe_2$ sample is tested by a femtosecond pulsed laser with central wavelength at 1560 nm, repetition rate of 28.7 MHz and pulse duration of 568 fs. The pump power is adjusted by a variable optical attenuator and separated at the ratio of 50:50 by an output coupler (OC). Two power meters are used to measure the output powers. Experimental and fitting results are depicted in Figure 4. Furthermore, by fitting the experimental results, the saturation intensity, modulation depth and nonsaturable absorbance are 22.67 MW/cm^2, 6.2 and 48.8%, respectively, based on the following classical equation [1–3]:

$$T(I) = 1 - \Delta T \cdot \exp(-I/I_{\mathrm{sat}}) - T_{\mathrm{ns}}$$

where $T(I)$ is transmission, I is input optical intensity, ΔT is modulation depth, I_{sat} is saturation intensity and T_{ns} is nonsaturable absorbance.

4 Experimental setup

The scheme of the $PdSe_2$-based passively mode-locked fiber laser is shown in Figure 5. A ring laser cavity is demonstrated. The gain medium is a piece of 9.1 m Er-doped fiber (ofs, MP980) with a peak absorption of ~6.5 dB/m at 1530 nm and a dispersion value of about −20 ps/(nm km) at 1550 nm. A 974-nm laser diode with a maximum output power of 680 mW is used as a pump source through a 980/1550 wavelength division multiplexer. A polarization independent isolator (PI-ISO) is employed as direction controller to ensure unidirectional delivery of the laser, and two polarization controllers (PCs) are used to adjust the polarization state and the loss in the cavity. In the experiment, mode-locked operations are more easily obtained by adjusting two PCs instead of one PC. The $PdSe_2$ SA is inserted between the PI-ISO and PC2. The 10% port of a 90:10 OC is used to export the laser. A piece of single-mode fiber (SMF) with a dispersion parameter of 18 ps/nm/km is added into the laser cavity for adjusting the net dispersion value of the laser cavity. Additionally, the output characteristics were recorded by an optical spectrum analyzer (AQ6317B, Yokogawa, Tokyo, Japan), a mixed oscilloscope (RTE1104, Rohde & Schwarz, Muenchen, Germany) connected with a 3 GHz high-speed InGaAs photodetector, a radio-frequency (RF) spectrum analyzer (FPC1000, Rohde & Schwarz, Muenchen, Germany), an optical power meter and an autocorrelator (FR-103XL, Femtochrome, Berkeley, America).

5 Results and discussion

5.1 Conventional soliton in anomalous dispersion cavity

In the experiment, firstly, for testing the absorption characteristics of the $PdSe_2$-PVA SA, the output performance of the fiber laser was investigated without using the SA. By carefully adjusting the rotation state of the PCs and the value of the pump power, only continuous-wave operation was detected. After that, the SA was inserted into the cavity and stable mode-locked pulse trains were emerged when the pump power was higher than 180 mW and the total

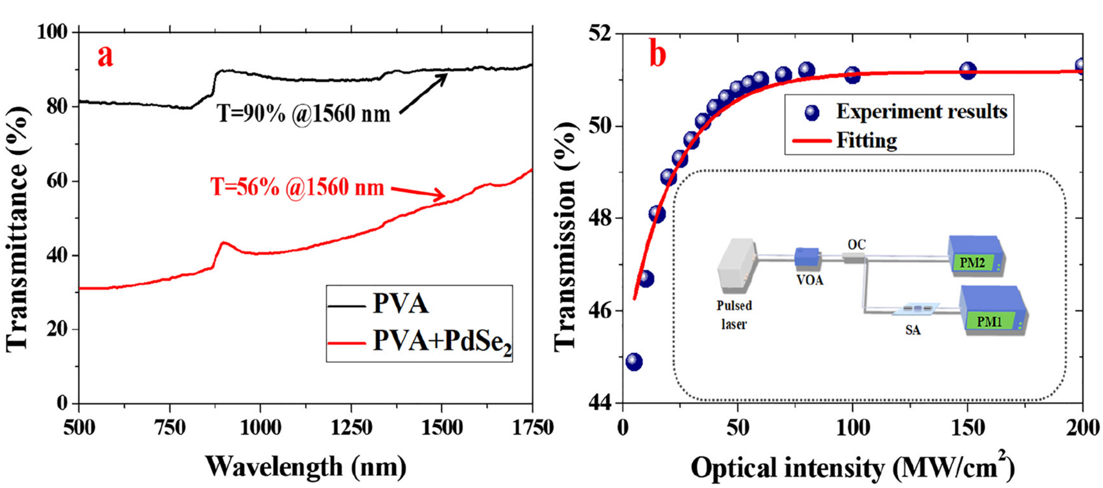

Figure 4: (a) Transmittance curves of the PVA and PVA-$PdSe_2$ SA. (b) Nonlinear transmission properties of the $PdSe_2$ SA under 1.5 μm source pumping. Insert of (b). The experimental setup used for testing nonlinear transmission properties. $PdSe_2$, palladium diselenide; SA, saturable absorber.

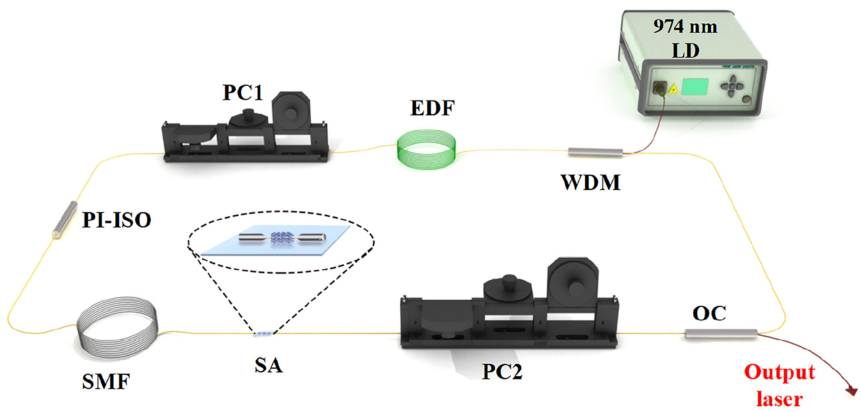

Figure 5: The scheme of the $PdSe_2$-based passively mode-locked fiber ring laser. $PdSe_2$, palladium diselenide.

cavity length was 26.65 m. Here, the net dispersion induced by the SMF and Er-doped fibers was about −0.15 ps^2, corresponding to anomalous dispersion region. The increased SMF compensated the net cavity dispersion into anomalous dispersion, which helped to produce the stable conventional mode-locked soliton. Kelly sidebands, the typical characteristics of the soliton laser, are shown in the optical emission spectrum in Figure 6(a), which are recorded by the optical spectrum analyzer at a resolution of 0.05 nm. However, Kelly sidebands obtained in our work are not as obvious as previous results obtained in conventional soliton operations [28, 29]. The formation of Kelly sidebands is due to the instability of modulation, which is related to the total laser gain, loss and dispersion value of the cavity. Thus, for different cavity demonstration, the Kelly sidebands exhibit distinct characteristics. As is shown, the central wavelength (λ_c) locates at 1533.61 nm, and the spectral full width at half maximum (FWHM) is measured to be 3.52 nm. Figure 6(b) depicts a typical pulse train of the $PdSe_2$-based Er-doped mode-locked laser, the pulse-to-pulse interval is 129.71 ns with a repetition frequency (f) of 7.71 MHz, matching well with the total cavity length of 26.65 m. The result indicates that the laser operates at a mode-locked state. The maximum average output power is 5.36 mW under the pump power of 436 mW, corresponding to a pulse energy of 0.70 nJ. The measured autocorrelation trace is provided in Figure 6(c). As is shown, the FWHM of the pulse is about 1.83 ps, assuming the pulse is the perfect $Sech^2$ type, and the real pulse width (τ) is about 1.19 ps. Combined with the 3 dB spectrum width of 3.52 nm, the time-bandwidth product (TBP) is calculated to be about 0.53. The TBP value is higher than the theoretical limit value, indicating that the conventional soliton is highly chirped, which is mainly attributed to the large dispersion value produced by the long length of the laser cavity. Large dispersion values will lead to a high-chirped soliton operation. Figure 6(d) is the RF spectrum recorded by a spectrum analyzer. As shown above, the RF spectrum is located at the fundamental frequency of 7.71 MHz, which was recorded with a bandwidth of 8 MHz and a resolution of 100 Hz. The signal-to-noise ratio (SNR) is about 55 dB. RF spectrum within 1 GHz width is also depicted in the insert of Figure 6(d) for further revealing its high stability characteristics. As is shown, all the results prove that the mode-locked pulses exhibit a high stability.

5.2 Dissipative soliton in normal dispersion cavity

For further testing the saturable absorption performance of the $PdSe_2$ SA in normal dispersion region, the net dispersion value of the laser cavity was adjusted to be about 0.16 ps^2 by adjusting the length of the laser cavity to be about 12.61 m, consisting 9.1 m erbium-doped fiber (EDF) and 3.51 m SMF. Under this condition, when the pump power was higher than 223 mW, stable mode-locked operation was recorded by adjusting the PCs. In normal dispersion region, the formation of dissipative soliton is due to the balance between the total laser gain and loss, the cavity dispersion, nonlinear optical effects and the birefringence filter effect induced by the PCs. Figure 7 shows the output characteristics of the $PdSe_2$-based mode-locked dissipative soliton operation. Emission optical spectrum with typical dissipative soliton characteristic of sharp steep edges is depicts in Figure 7(a). The central wavelength is 1560.67 nm; meanwhile, the FWHM is as broad as 35.37 nm. The pulse-to-pulse interval of the typical pulse train (Figure 7(b)) is about 61.39 ns, corresponding to a cavity length–dependent pulse repetition rate of 16.29 MHz, indicating that the mode-locked operation is on fundamental frequency state. The pulse width characteristics are also investigated and shown in Figure 7(c). The FWHM of the pulse is about 21.1 ps. Considering a Gaussian fitting for dissipative soliton, the real pulse duration is calculated to be about 14.92 ps (21.1 × 0.707 ps). Thus, the TBP of the

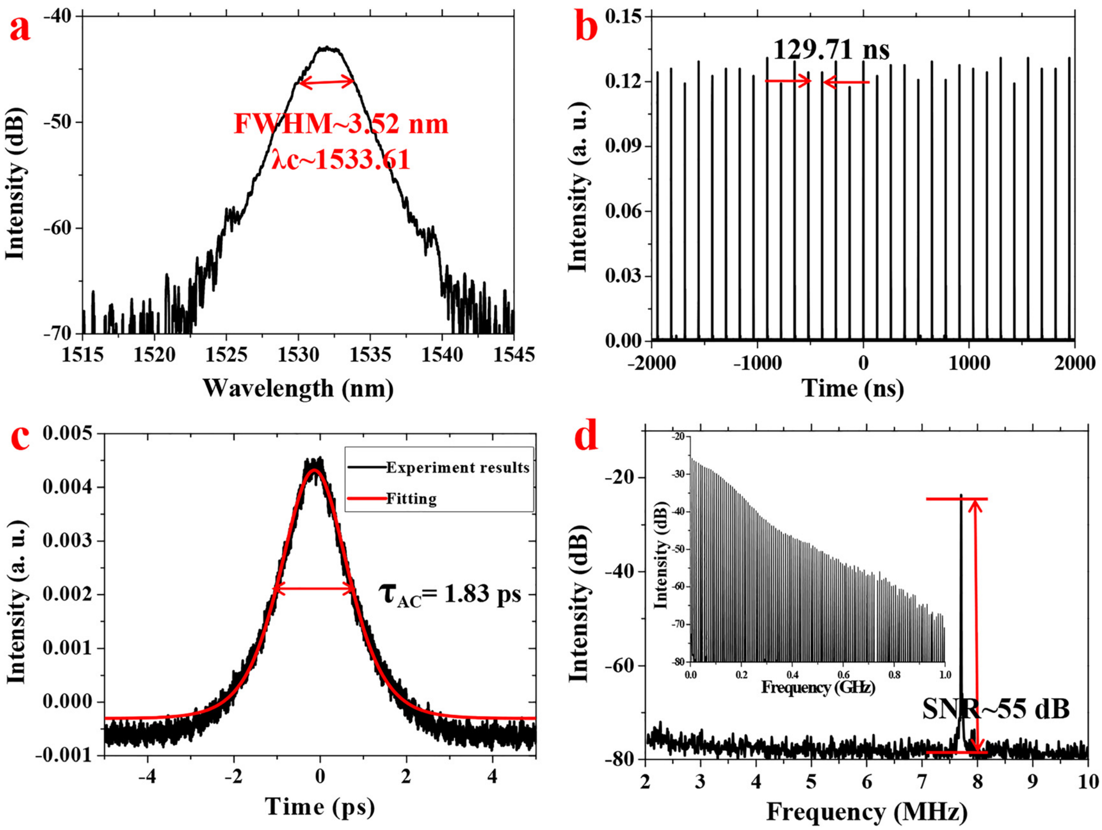

Figure 6: Output characteristics of the conventional soliton operation.
(a) Emission optical spectrum. (b) Typical pulse train. (c) Measured autocorrelation trace. (d) RF spectrum located at fundamental frequency. Insert of (d) RF spectrum within 1 GHz. RF, radio-frequency.

dissipative soliton is about 65. Large TBP value proves that the pulses are of large frequency chirp which is due to the combined effects of normal dispersion and fiber nonlinearity. The RF spectrum located at the fundamental frequency of 16.29 MHz with an SNR of about 75 dB is depicted in Figure 7(d). The insert of Figure 7(d) gives the wide band RF spectrum of the mode-locked operation, which proves that the dissipative soliton operation exhibits excellent stability. In comparison with the conventional soliton operation, the stability enhancement of the dissipative soliton operation is mainly due to the increase of the output power acting as signal. The maximum average output power (P_{ave}) of the dissipative soliton operation is as high as 46.67 mW under the maximum pump power of 620 mW, corresponding to an optical-to-optical conversion efficiency of 7.53% and a maximum pulse energy (E_p) of 2.86 nJ, which also exhibits obvious enhancement in comparison with previous works [24, 25, 29–31, 52]. Also, in our work, in comparison with the conventional soliton operation, the maximum output power and pulse energy of the dissipative soliton operation are all higher. Because the pulse energy of dissipative soliton is not limited by the theory of soliton area, meanwhile, the pulse energy of conventional soliton is limited to be 0.1 nJ level. In addition, as is reported, dissipative soliton also exhibits vector characteristics [69], and its pulse width can be compressed by adding a piece of SMF outside the cavity. Our future work will also study its vector and compression characteristics. Besides, as described, a 10:90 OC was used for outputting the pulse energies through its 10% port. The output energy is 2.86 nJ, corresponding to an intracavity pulse energy of 25.74 nJ. Thus, the intracavity optical intensity can be calculated to be about 2.72 GW/cm^2; due to limitation of the pump power, the exact damage threshold of the $PdSe_2$ SA is not measured; however, the threshold is higher than 2.72 GW/cm^2, which guarantees the generations of high-power and large-energy soliton operations.

Additionally, the threshold powers of the conventional and dissipative soliton are 180 and 223 mW, respectively, which are higher than the results obtained in previous reported 2D material–based mode-locked fiber laser operations [19, 20, 24–26]. Because, the non-saturable absorbance of the $PdSe_2$ SA was 48.8%, corresponding to a

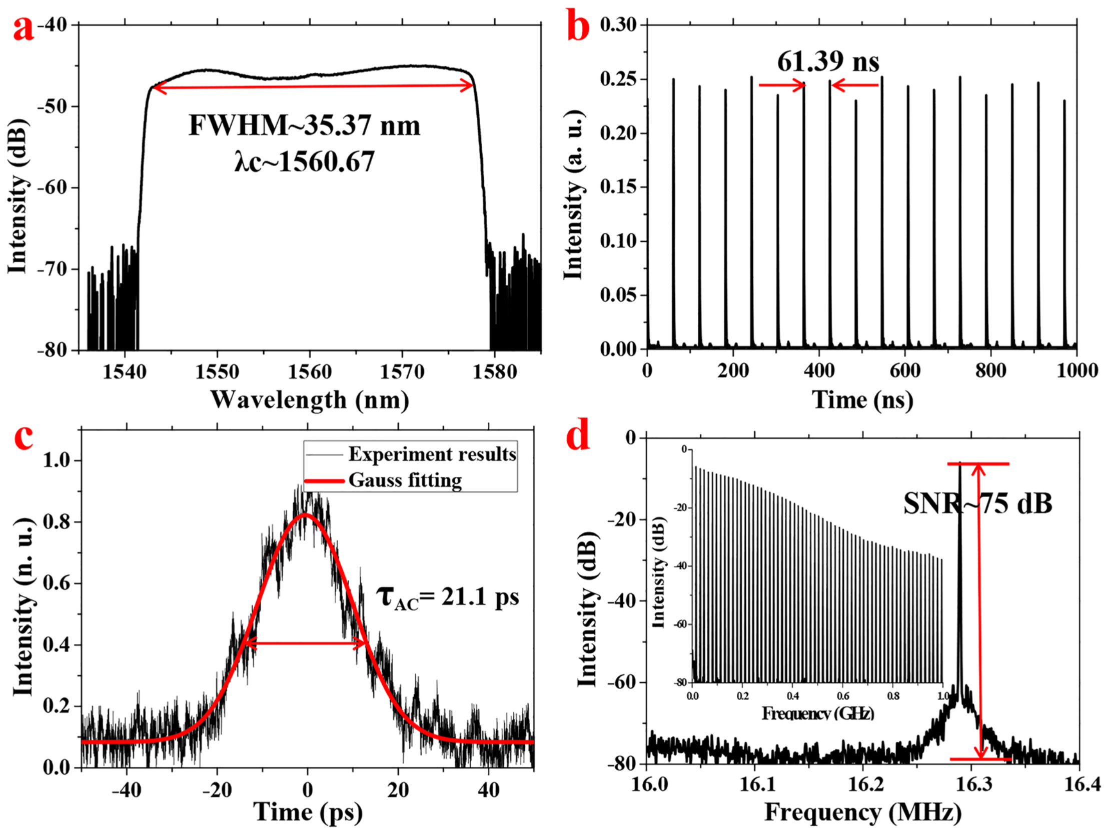

Figure 7: Output characteristics of the dissipative soliton operation.
(a) Emission optical spectrum. (b) Typical pulse train. (c) Measured autocorrelation trace. (d) RF spectrum located at fundamental frequency. Insert of (d) RF spectrum within 1 GHz. RF, radio-frequency.

insert loss of about 2.9 dB, large insert loss will lead to a high threshold power of the mode-locked laser. In addition, large insert loss or high threshold power will produce serious thermal effects, which will affect the stability of the pulse and result in pulse fluctuation (shown in Figures 6(b) and 7(b)). Thus, in the future work, we will commit to the preparation of $PdSe_2$ SAs with low insert loss by optimizing the preparation parameters.

5.3 Comparison of output laser characteristics

5.3.1 Comparison of dissipative soliton operations

2D layered materials have significantly promoted the investigation progress of various optical solitons including conventional soliton, dissipative soliton, dark soliton and so on. Among which, dissipative soliton exhibits obvious competitive advantages of large pulse energy and high peak power. However, in comparison with the common reported conventional soliton operations, investigations on 2D material–based dissipative soliton operations are still far from thoroughly investigated. Table 1 gives a relatively comprehensive comparison of the output performance of 2D material–based mode-locked dissipative soliton lasers. As is shown, 2D materials including graphene [15], TMDs [24–26], TIs [19, 20], Xenes [45] and so on have been employed as SAs for generating dissipative soliton operations. From the comparison, the maximum average output power and pulse energy were obtained in our work. Additionally, the spectrum width obtained in our work is as broad as 35.37 nm, which is competitive in comparison with the previous works. Such broad spectrum width fully revealed the capacity of our laser in obtaining fs-level ultrafast pulses through extracavity compression.

5.3.2 Comparison of conventional soliton operations

Besides the mentioned 2D materials, well-known non-2D crystals including QDs [6, 70], nanoparticles [71–73] and nanorods [74] also have been used for demonstrating mode-locked fiber laser operations, especially, for

Table 1: Comparison of 2D material–based mode-locked dissipative soliton operations.

SA	$I_{sat}/\Delta T$ (MW cm^{-2}/%)	λ_c (nm)	FWHM (nm)	P_{ave} (mW)	τ (ps)	f (MHz)	E_p (nJ)	Ref
Graphene	0.71/–	–	7.2	–	49	–	–	[15]
MoS_2	8000/4.4	1596	9.4	1.8	121	3.63	0.5	[24]
WS_2	–/5.1	1565.5	14.5	1.8	21.1	8.05	0.22	[25]
SnS_2	118/5.4	1560	31	14.2	152 fs	29.6	0.48	[26]
Sb_2Te_3	–/5.3	1558	34	5.34	167 fs	25.38	0.21	[19]
Bi_2Te_3	6.48/10.39	1571	39.95	11	4.72	10.71	1.03	[20]
Tellurene	34.3/5.06	1574	18.1	23.61	5.87	12.17	1.94	[45]
$PdSe_2$	22.67/6.2	1560.7	35.37	46.67	14.92	16.29	2.86	Our

SA, saturable absorber.

Table 2: Comparison of non-2D crystal–based mode-locked conventional soliton operations and our work.

SA	$I_{sat}/\Delta T$ (MW.cm^{-2}/%)	λ_c (nm)	FWHM (nm)	P_{ave} (mW)	τ (ps)	f (MHz)	E_p (nJ)	Ref
PbS/CdS QD	6.29/4.95	1562.5	2.504	2.71	54	3.302	0.82	[6]
Phosphorene QD	–/18.1	1561.7	3	0.135	0.882	5.47	0.025	[70]
ITO nanoparticle	11.9/8.3	1558.5	0.27	–	1.67 ns	1.96	–	[71]
NiO nanoparticle	0.04/39	1561.8	2.85	1.09	0.95	0.96	1.14	[72]
Fe_3O_4 nanoparticle	21.12/7.4	1558	0.8	17	4.35 ns	37.32	0.46	[73]
Gold nanorods	1.05/4.4	1561	1.17	2.05	12	34.7	0.059	[74]
$PdSe_2$	22.67/6.2	1533.61	3.52	5.36	1.19	7.71	0.7	Our

SA, saturable absorber; QD, quantum dot.

obtaining conventional soliton operations. Comparison of the output characteristics of non-2D crystal–based mode-locked fiber lasers and our work is depicted in Table 2. As is shown, in comparison with non-2D crystal–based SAs, $PdSe_2$ SA used in our work exhibits larger saturation intensity. And our work also exhibits competitive output laser characteristics including wide FWHM, high output power, short pulse width and large pulse energy. All the results depicted in Tables 1 and 2 prove that the $PdSe_2$ SA exhibits competitive nonlinear optical absorption properties and excellent performance in acting as ultrafast photonics devices.

5.4 Saturable absorption mechanism of 2D material–based photonics devices

For 2D material–based photonics devices, its saturable absorption mechanism can be explained by subbandgap absorption or Pauli blocking principle [1, 27, 42, 45]. As is shown in Figure 8, the bandgap value of 2D material can be defined as ΔE. When the energy of the incident light is lower than ΔE, the incident light cannot be absorbed directly. Meanwhile, subbandgap absorption, defects in the materials and two-photon absorption will be applied for explaining the absorption [42, 44]. Besides, when the

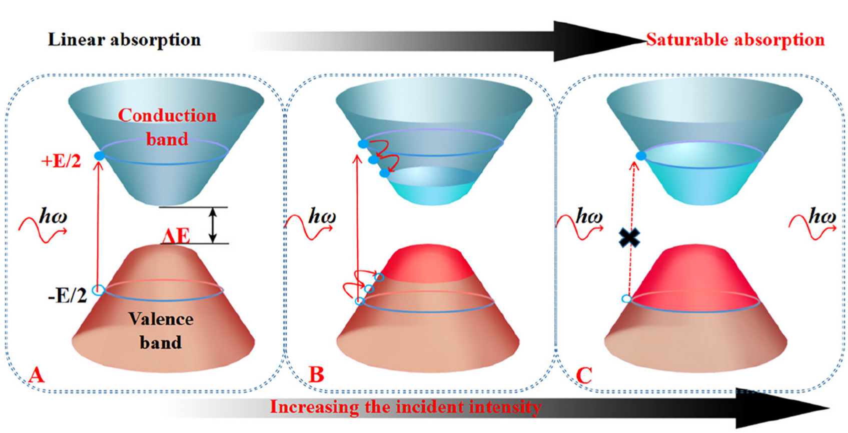

Figure 8: Saturable absorption mechanism explained by Pauli blocking principle.

energy of the incident light is larger than ΔE, the saturable absorption mechanism is explained by Pauli blocking principle [42, 45]. The absorption progress is depicted in Figure 8. Firstly, linear absorption occurs under low incident light intensity. In detail, electrons distributed in the valence band absorb the energy of the incident light and be excited into the conduction band. After that, Fermi-Dirac distribution with newly created electron-hole pairs will form due to the fact that hot electrons cooled almost immediately, which will lead to the absorption of photons. Finally, electrons and holes recombine and reach to an equilibrium distribution state due to the intraband phonon scattering. However, under a higher incident optical intensity, saturable absorption will occurred because the energy states near the edge will be filled due to the high concentration of photocarriers. Under this condition, the absorption will be blocked and the photons will transmit the material without absorption. Based on the discussion, the ΔE of 2D materials, deciding the absorption mechanism, exhibits great significance in designing ultrafast photonics devices. Additionally, the $PdSe_2$ nanosheets used in our experiment exhibit about 15–16 layers and a corresponding narrow bandgap value of 0.02 eV. The energy of the mode-locked operation is about 0.8 eV, indicating that saturable absorption contributes to the modulation application in our work.

6 Conclusion

In conclusion, electronic band structures, bandgap characteristics, preparation and nonlinear optical properties of $PdSe_2$ are investigated theoretically and experimentally. Based on the $PdSe_2$ SA, conventional and dissipative soliton operations were obtained within Er-doped fiber lasers. Conventional soliton with a 1.19 ps pulse width under a repetition rate of 7.71 MHz was obtained within anomalous dispersion region. Meanwhile, based on normal dispersion laser cavity, dissipative soliton operation with a 46.67 mW maximum average output power, 35.37 nm spectrum width and 2.86 nJ pulse energy was generated successfully. The competitive results present the capacity of $PdSe_2$ in designing broadband ultrafast optical devices, which also provide meaningful reference for designing 2D material–based ultrafast photonic devices.

Acknowledgment: This work was supported by the National Science Foundation (NSF) (61971271, 11904213, 11747149), Shandong Province Natural Science Foundation (ZR2018QF006), the Taishan Scholars Project of Shandong Province (Tsqn20161023), Primary Research and Development Plan of Shandong Province (2018GGX101018) and 'Opening Foundation of Shandong Provincial Key Laboratory of Laser Technology and Application'.

Author contribution: All authors have accepted responsibility for the entire content of this submitted manuscript and approved its submission.

Research funding: This work was supported by the National Science Foundation (NSF) (61971271, 11904213, 11747149), Shandong Province Natural Science Foundation (ZR2018QF006), the Taishan Scholars Project of Shandong Province (Tsqn20161023), Primary Research and Development Plan of Shandong Province (2018GGX101018) and `Opening Foundation of Shandong Provincial Key Laboratory of Laser Technology and Application'.

Conflict of interest statement: The authors declare no conflicts of interest regarding this article.

References

[1] B. Guo, Q. L. Xiao, S. H. Wang, et al., "2D layered materials: synthesis, nonlinear optical properties, and device applications," *Laser Photonics Rev.*, vol. 13, p. 1800327, 2019.
[2] S. Y. Guo, Y. P. Zhang, Y. Q. Ge, et al., "2D V-V binary materials: status and challenges," *Adv. Mater.*, vol. 31, p. 1902352, 2019.
[3] Y. F. Song, X. J. Shi, C. F. Wu, et al., "Recent progress of study on optical solitons in fiber lasers," *Appl. Phys. Rev.*, vol. 6, 2019, Art no. 021313.
[4] W. J. Liu, M. L. Liu, X. M. Liu, et al., "Recent advances of 2D materials in nonlinear photonics and fiber lasers," *Adv. Opt. Mater.*, vol. 8, p. 1901631, 2020.
[5] H. N. Zhang, and J. Liu, "Gold nanobipyramids as saturable absorbers for passively Q-switched laser generation in the 1.1 μm region," *Opt. Lett.*, vol. 41, pp. 1150–1152, 2016.
[6] N. Ming, S. N. Tao, W. Q. Yang, et al., "Mode-locked Er-doped fiber laser based on PbS/CdS core/shell quantum dots as saturable absorber," *Opt. Express*, vol. 26, pp. 9017–9026, 2018.
[7] L. Yun, Y. Qiu, C. H. Yang, et al., "PbS quantum dots as a saturable absorber for ultrafast laser," *Photonics Res.*, vol. 6, pp. 1028–1032, 2018.
[8] A. Martinez, K. Fuse, and S. Yamashita, "Enhanced stability of nitrogen-sealed carbon nanotube saturable absorbers under high-intensity irradiation," *Opt. Express*, vol. 21, pp. 4665–4670, 2013.
[9] J. H. Im, S. Y. Choi, F. Rotermund, et al., "All-fiber Er-doped dissipative soliton laser based on evanescent field interaction with carbon nanotube saturable absorber," *Opt. Express*, vol. 18, pp. 22141–22146, 2010.
[10] G. Steinmeyer, D. H. Sutter, L. Gallmann, et al., "Frontiers in ultrashort pulse generation: pushing the limits in linear and nonlinear optics," *Science*, vol. 286, pp. 1507–1512, 1999.
[11] U. Keller, "Recent developments in compact ultrafast lasers," *Nature*, vol. 424, pp. 831–838, 2003.

[12] Q. L. Bao, H. Zhang, Y. Wang, et al., "Atomic-layer graphene as a saturable absorber for ultrafast pulsed lasers," *Adv. Funct. Mater.*, vol. 19, pp. 3077–3083, 2009.

[13] Z. P. Sun, T. Hasan, F. Torrisi, et al., "Graphene mode-locked ultrafast laser," *ACS Nano*, vol. 4, pp. 803–810, 2010.

[14] H. Zhang, Q. L. Bao, D. Y. Tang, et al., "Large energy soliton erbium-doped fiber laser with a graphene-polymer composite mode locker," *Appl. Phys. Lett.*, vol. 95, p. 141103, 2009.

[15] H. Zhang, D. Y. Tang, R. J. Knize, et al., "Graphene mode locked, wavelength-tunable, dissipative soliton fiber laser," *Appl. Phys. Lett.*, vol. 96, p. 111112, 2010.

[16] M. Jung, J. Koo, J. Park, et al., "Mode-locked pulse generation from an all-fiberized, Tm-Ho-codoped fiber laser incorporating a graphene oxide-deposited side-polished fiber," *Opt. Express*, vol. 21, pp. 20062–20072, 2013.

[17] C. J. Zhao, H. Zhang, X. Qi, et al., "Ultra-short pulse generation by a topological insulator based saturable absorber," *Appl. Phys. Lett.*, vol. 101, p. 211106, 2012.

[18] N. N. Xu, N. Ming, X. L. Han, et al., "Large-energy passively Q-switched Er-doped fiber laser based on CVD-Bi_2Se_3 as saturable absorber," *Opt. Mater. Express*, vol. 9, pp. 373–383, 2019.

[19] J. Boguslawski, G. Sobon, R. Zybala, et al., "Dissipative soliton generation in Er-doped fiber laser mode-locked by Sb_2Te_3 topological insulator," *Opt. Lett.*, vol. 40, pp. 2786–2789, 2015.

[20] Q. K. Wang, Y. Chen, L. L. Miao, et al., "Wide spectral and wavelength-tunable dissipative soliton fiber laser with topological insulator nano-sheets self-assembly films sandwiched by PMMA polymer," *Opt. Express*, vol. 23, pp. 7681–7693, 2015.

[21] K. P. Wang, J. Wang, J. T. Fan, et al., "Ultrafast saturable absorption of two-dimensional MoS_2 nanosheets," *ACS Nano*, vol. 7, pp. 9260–9267, 2013.

[22] H. Zhang, S. B. Lu, J. Zheng, et al., "Molybdenum disulfide (MoS_2) as a broadband saturable absorber for ultra-fast photonics," *Opt. Express*, vol. 22, pp. 7249–7260, 2014.

[23] H. N. Zhang, P. F. Ma, M. X. Zhu, et al., "Palladium selenide as a broadband saturable absorber for ultra-fast photonics," *Nanophotonics*, vol. 9, no. 8, pp. 2557–2567, 2020.

[24] Y. D. Cui, F. F. Lu, and X. M. Liu, "MoS_2-clad microfibre laser delivering conventional, dispersion-managed and dissipative solitons," *Sci. Rep.*, vol. 6, pp. 1–8, 2016.

[25] D. Mao, S. L. Zhang, Y. D. Wang, et al., "WS_2 saturable absorber for dissipative soliton mode locking at 1.06 and 1.55 μm," *Opt. Express*, vol. 23, pp. 27509–27519, 2015.

[26] S. Li, Y. Yin, Q. Y. Ouyang, et al., "Dissipative soliton generation in Er-doped fibre laser using SnS_2 as a saturable absorber," *Appl. Phys. Express*, vol. 12, p. 102008, 2019.

[27] K. D. Niu, R. Y. Sun, Q. Y. Chen, et al., "Passively mode-locked Er-doped fiber laser based on SnS_2 nanosheets as a saturable absorber," *Photonics Res*, vol. 6, pp. 72–76, 2018.

[28] L. Li, L. H. Pang, Q. Y. Zhao, et al., "VSe_2 nanosheets for ultrafast fiber lasers," *J. Mater. Chem. C*, vol. 8, pp. 1104–1109, 2020.

[29] L. Li, L. H. Pang, Q. Y. Zhao, et al., "Niobium disulfide as a new saturable absorber for an ultrafast fiber laser," *Nanoscale*, vol. 12, pp. 4537–4543, 2020.

[30] J. S. Liu, X. H. Li, Y. X. Guo, et al., "$SnSe_2$ nanosheets for femtosecond harmonic mode-locked pulse generation," *Small*, vol. 15, p. 1902811, 2019.

[31] J. J. Feng, X. H. Li, Z. J. Shi, et al., "2D ductile transition metal chalcogenides (TMCs): a novel high-performance Ag_2S nanosheets for ultrafast photonics," *Adv. Opt. Mater.*, vol. 8, p. 1901762, 2019.

[32] P. F. Ma, J. S. Li, H. N. Zhang, et al., "Preparation of high-damage threshold WS_2 modulator and its application for generating high-power large-energy bright-dark solitons," *Infrared Phys. Technol.*, vol. 105, p. 103257, 2020.

[33] K. D. Niu, Q. Y. Chen, R. Y. Sun, et al., "Passively Q-switched erbium-doped fiber laser based on SnS_2 saturable absorber," *Opt. Mater. Express*, vol. 7, pp. 3934–3943, 2017.

[34] Q. Y. Hu, X. Y. Zhang, Z. J. Liu, et al., "High-order harmonic mode-locked Yb-doped fiber laser based on a $SnSe_2$ saturable absorber," *Opt. Laser Technol.*, vol. 119, p. 105639, 2019.

[35] Y. Chen, G. B. Jiang, S. Q. Chen, et al., "Mechanically exfoliated black phosphorus as a new saturable absorber for both Q-switching and mode-locking laser operation," *Opt. Express*, vol. 23, pp. 12823–12833, 2015.

[36] X. M. Wang, and S. F. Lan, "Optical properties of black phosphorus," *Adv. Opt. Photon*, vol. 8, pp. 618–655, 2016.

[37] M. Zhang, Q. Wu, F. Zhang, et al., "2D black phosphorus saturable absorbers for ultrafast photonics," *Adv. Optical Mater.*, vol. 7, p. 1800224, 2019.

[38] Y. I. Jhon, J. Koo, B. Anasori, et al., "Metallic MXene saturable absorber for femtosecond mode-locked lasers," *Adv. Mater.*, vol. 29, p. 1702496, 2017.

[39] X. T. Jiang, S. X. Liu, W. Y. Liang, et al., "Broadband nonlinear photonics in few-layer MXene $Ti_3C_2T_x$ (T= F, O, or OH)," *Laser Photonics Rev.*, vol. 12, p. 1700229, 2018.

[40] Y. F. Song, Z. M. Liang, X. T. Jiang, et al., "Few-layer antimonene decorated microfiber: ultra-short pulse generation and all-optical thresholding with enhanced long term stability," *2D Mater.*, vol. 4, 2017, Art no. 045010.

[41] L. Lu, Z. M. Liang, L. M. Wu, et al., "Few-layer bismuthene: sonochemical exfoliation, nonlinear optics and applications for ultrafast photonics with enhanced stability," *Laser Photonics Rev.*, vol. 12, p. 1700221, 2018.

[42] B. Guo, S. H. Wang, Z. X. Wu, et al., "Sub-200 fs soliton mode-locked fiber laser based on bismuthene saturable absorber," *Opt. Express*, vol. 26, pp. 22750–22760, 2018.

[43] C. Wang, L. Wang, X. H. Li, et al., "Few-layer bismuthene for femtosecond soliton molecules generation in Er-doped fiber laser," *Nanotechnology*, vol. 30, 2018, Art no. 025204.

[44] J. Guo, J. L. Zhao, D. Z. Huang, et al., "Two-dimensional tellurium-polymer membrane for ultrafast photonics," *Nanoscale*, vol. 11, pp. 6235–6242, 2019.

[45] N. N. Xu, P. F. Ma, S. G. Fu, et al., "Tellurene-based saturable absorber to demonstrate large-energy dissipative soliton and noise-like pulse generations," *Nanophotonics*, vol. 1, 2020. https://doi.org/10.1515/nanoph-2019-0545.

[46] Q. H. Wang, K. Kalantar-Zadeh, A. Kis, et al., "Electronics and optoelectronics of two-dimensional transition metal dichalcogenides," *Nat. Nanotechnol.*, vol. 7, pp. 699–712, 2012.

[47] F. N. Xia, H. Wang, D. Xiao, et al., "Two-dimensional material nanophotonics," *Nat Photonics*, vol. 8, pp. 899–907, 2014.

[48] K. P. Wang, J. Wang, J. T. Fan, et al., "Ultrafast saturable absorption of two-dimensional MoS_2 nanosheets," *ACS Nano*, vol. 7, pp. 9260–9267, 2013.

[49] J. F. Sun, H. L. Shi, T. Siegrist, et al., “Electronic, transport, and optical properties of bulkand mono-layer $PdSe_2$,” *Appl. Phys. Lett.*, vol. 107, p. 153902, 2015.
[50] A. D. Oyedele, S. Z. Yang, L. B. Liang, et al., “$PdSe_2$: pentagonal two-dimensional layers with high air stability for electronics,” *J. Am. Chem. Soc.*, vol. 139, pp. 14090–14097, 2017.
[51] L. H. Zeng, D. Wu, S. H. Lin, et al., “Controlled synthesis of 2D palladium diselenide for sensitive photodetector applications,” *Adv. Funct. Mater.*, vol. 29, p. 1806878, 2019.
[52] E. Li, D. F. Wang, P. Fan, et al., “Construction of bilayer $PdSe_2$ on epitaxial graphene,” *Nano Res.*, vol. 11, pp. 5858–5865, 2018.
[53] A. A. Puretzky, A. D. Oyedele, K. Xiao, et al., “Anomalous interlayer vibrations in strongly coupled layered PdSe2,” *2D Mater.*, vol. 5, 2018, Art no. 035016.
[54] W. L. Chow, P. Yu, F. C. Liu, et al., “High mobility 2D palladium diselenide field-effect transistors with tunable ambipolar characteristics,” *Adv. Mater.*, vol. 29, p. 1602969, 2017.
[55] M. S. Long, Y. Wang, P. Wang, et al., “Palladium diselenide long-wavelength infrared photodetector with high sensitivity and stability,” *ACS Nano*, vol. 13, pp. 2511–2519, 2019.
[56] Y. Wang, Y. F. Li, and Z. F. Chen, “Not your familiar two dimensional transition metal disulfide: structural and electronic properties of the PdS_2 monolayer,” *J. Mater. Chem. C*, vol. 3, pp. 9603–9608, 2015.
[57] F. Y. Li, K. X. Tu, H. J. Zhang, et al., “Flexible structural and electronic properties of a pentagonal B_2C monolayer via external strain: a computational investigation,” *Phys. Chem. Chem. Phys.*, vol. 17, pp. 24151–24156, 2015.
[58] A. Lopez-Bezanilla, P. B. Littlewood. “σ–π-band inversion in a novel two-dimensional material,” *J. Phys. Chem. C*, vol. 119, pp. 19469–19474, 2015.
[59] Y. Ding, Y. L. Wang, “Hydrogen-induced stabilization and tunable electronic structures of penta-silicene: a computational study,” *J. Mater. Chem. C*, vol. 3, pp. 11341–11348, 2015.
[60] J. Xiao, M. Q. Long, C. S. Deng, et al., “Electronic structures and carrier mobilities of blue phosphorus nanoribbons and nanotubes: a first-principles study,” *J. Phys. Chem. C*, vol. 120, pp. 4638–4646, 2016.
[61] X. B. Liu, H. C. Zhou, B. Yang, et al., “Strain-modulated electronic structure and infrared light adsorption in palladium diselenide monolayer,” *Sci. Rep.*, vol. 7, pp. 1–6, 2017.
[62] A. D. Oyedele, S. Z. Yang, T. L. Feng, et al., “Defect-mediated phase transformation in anisotropic two-dimensional $PdSe_2$ crystals for seamless electrical contacts,” *J. Am. Chem. Soc.*, vol. 141, pp. 8928–8936, 2019.
[63] G. D. Nguyen, A. D. Oyedele, A. Haglund, et al., “Atomically precise $PdSe_2$ pentagonal nanoribbons,” *ACS Nano*, vol. 14, pp. 1951–1957, 2020.
[64] Y. Y. Gu, H. Cai, J. C. Dong, et al., “Two-dimensional palladium diselenide with strong in-plane optical anisotropy and high mobility grown by chemical vapor deposition,” *Adv. Mater.*, vol. 32, p. 1906238, 2020.
[65] J. P. Perdew, and A. Zunger, “Self-interaction correction to density functional approximation for many-electron systems,” *Phys. Rev. B*, vol. 23, p. 5048, 1981.
[66] G. Kresse, and D. Joubert, “From ultrasoft pseudopotentials to the projector augmented-wave method,” *Phys. Rev. B*, vol. 59, p. 1758, 1999.
[67] J. P. Perdew, K. Burke, and M. Ernzerhof, “Generalized gradient approximation made simple,” *Phys. Rev. Lett.*, vol. 77, p. 3865, 1996.
[68] J. Klimeš, D. R. Bowler, and A. Michaelides, “Chemical accuracy for the van der Waals density functional,” *J. Phys. Condens. Matter*, vol. 22, 2009, Art no. 022201.
[69] L. Yun, “Generation of vector dissipative and conventional solitons in large normal dispersion regime,” *Opt. Express*, vol. 25, pp. 18751–18759, 2017.
[70] J. Du, M. Zhang, Z. Guo, et al., “Phosphorene quantum dot saturable absorbers for ultrafast fiber lasers,” *Sci. Rep.*, vol. 7, p. 42357, 2017.
[71] Q. X. Guo, J. Pan, D. W. Li, et al., “Versatile mode-locked operations in an er-doped fiber laser with a film-type indium tin oxide saturable absorber,” *Nanomaterials*, vol. 9, p. 701, 2019.
[72] A. Nady, M. H. M. Ahmed, A. A. Latiff, et al., “Femtoseconds soliton mode-locked erbium-doped fiber laser based on nickel oxide nanoparticle saturable absorber,” *Chin. Opt. Lett.*, vol. 10, pp. 32–36, 2017.
[73] N. Li, H. Jia, J. X. Liu, et al., “Fe_3O_4 nanoparticles as the saturable absorber for a mode-locked fiber laser at 1558 nm,” *Laser Phys. Lett.*, vol. 16, 2019, Art no. 065102.
[74] Z. Kang, Y. Xu, L. Zhang, et al., “Passively mode-locking induced by gold nanorods in erbium-doped fiber lasers,” *Appl. Phys. Lett.*, vol. 103, pp. 0411051–0411054, 2013.